Use of Field-Induced Surface-Organometallic Interactions to Control Selectivity in Rhodium-Catalyzed Organic Reaction

Dylan Barber
Chemistry Major, Williams College

NNIN REU Site: Stanford Nanofabrication Facility, Stanford University, Stanford, CA
NNIN REU Principal Investigator: Professor Matthew Kanan, Chemistry Department, Stanford University
NNIN REU Mentor: Craig Gorin, Chemistry Department, Stanford University
Contact: dylan.m.barber@williams.edu, mkanan@stanford.edu, cgorin@stanford.edu

Abstract:

A major challenge facing chemists is to control the selectivity of chemical reactions. The common response is to focus entirely on catalyst design to improve yields of desired products. Electric fields generated at the interface of an electrode and electrolyte solution have shown promise as an additional method to control chemical reactions. In previous work, our group showed that Lewis acid-catalyzed rearrangements of epoxides favor different products when subjected to interfacial electric fields [1]. It was also established that interfacial electric fields can induce surface-organometallic interactions that can change product ratios in a rhodium-catalyzed carbene reaction more than 100-fold [2]. In this work, we exploited a field-induced TiO_2-rhodium porphyrin interaction to change the site selectivity of a C-H insertion reaction (Figure 1). Depending on the interfacial charge density, the product ratio in the rhodium porphyrin-catalyzed reaction of 1-diazo-3-(3-methoxyphenyl) propan-2-one (1) to 5-methoxy-1*H*-inden-2(3*H*)-one (2) and 4-methoxy-1*H*-inden-2(3*H*)-one (3) changes 16-fold, with a 3.6-fold increase in conversion of the starting material. We also investigated alternative HfO_2 and Ta_2O_5 dielectrics, which showed similar field-induced selectivity effects.

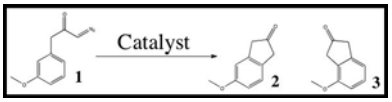

*Figure 1: Reaction scheme for conversion of 1-diazo-3-(3-methoxyphenyl)propan-2-one (1) to 5-methoxy-1*H*-inden-2(3*H*)-one (2) and 4-methoxy-1*H*-inden-2(3*H*)-one (3).*

Introduction:

Chemists can exert substantial control over the selectivity of many reactions by changing the steric and electronic properties of the relevant catalyst, but very little is known about the impact of certain environmental factors on catalytic selectivity. Specifically, the application of an electric field has the potential to affect selectivity in chemical reactions by stabilizing aligned transition-state dipolar species, lowering the activation barrier towards—and altering selectivity in favor of—the associated product. In the model reaction cell outlined in Figure 2, an applied potential induces the formation of an electric field at the interface between a charged dielectric surface and the contiguous electrolyte solution.

Using a catalyst fixed to the dielectric surface by intermolecular forces, previous work by our group has shown two interesting results. First, electric fields can change the selectivity of certain chemical reactions. Second—in the case of a rhodium porphyrin-catalyzed carbene reaction—an electric field can induce an interaction between the catalyst and a titanium dioxide (TiO_2) dielectric. This result is interesting because the selectivity change was in the opposite direction to that shown on an aluminum oxide (Al_2O_3) dielectric under otherwise identical conditions. This and other experiments conducted in the same study indicated an electric field-induced interaction between a TiO_2 dielectric surface and the rhodium porphyrin catalyst that could potentially be used to control selectivity in other reactions [2].

The purpose of this study is to further investigate this electric field-induced catalyst-dielectric interaction by examining a carbene insertion reaction (Figure 1) using a rhodium porphyrin catalyst on aluminum oxide, titanium oxide, and other dielectric surfaces.

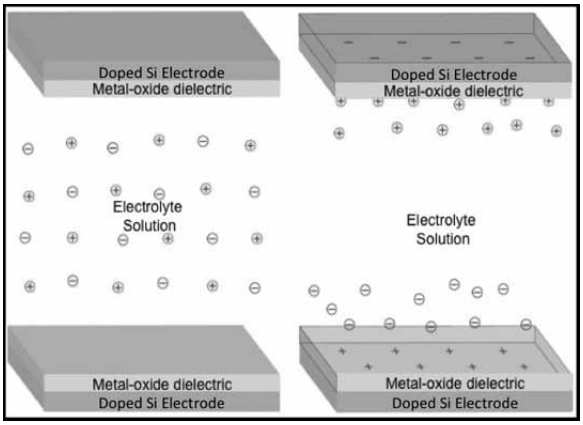

Figure 2: Model of the reaction cell used in this study. Left: a neutral reaction cell. Right: a reaction cell with applied potential, forming a localized electric field at each dielectric surface.

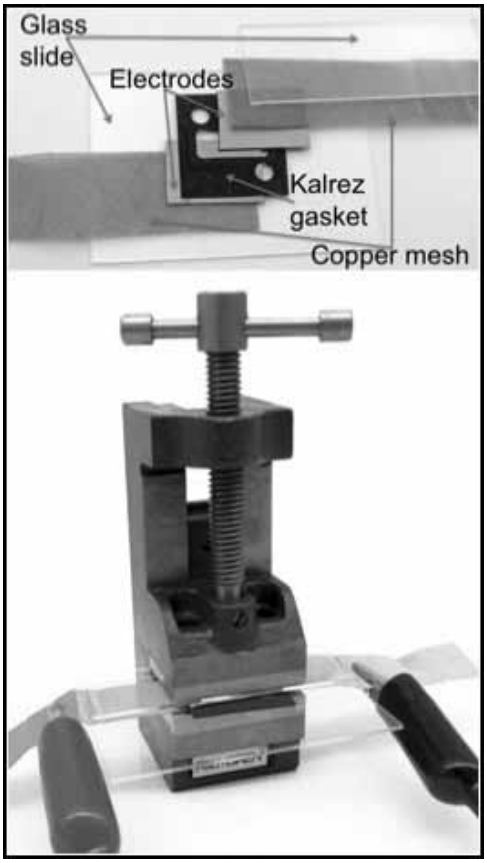

Figure 3: The parallel plate cell.

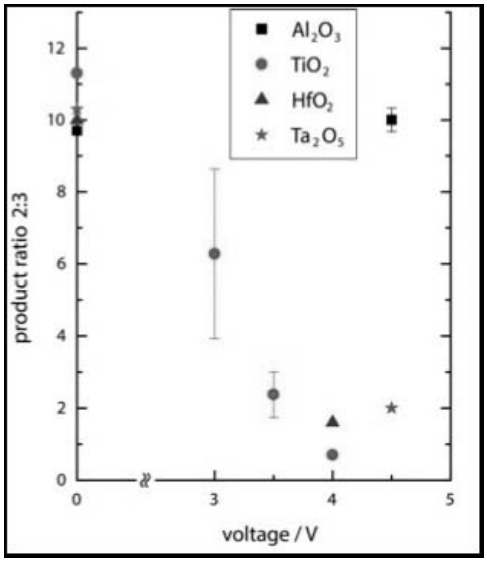

*Figure 4: Product ratio **2:3** as a function of applied voltage on Al_2O_3, TiO_2, HfO_2, and Ta_2O_5 dielectrics.*

Experimental Procedure:

Using atomic layer deposition (ALD), 50Å of metal oxide were deposited on highly doped silicon wafers. The wafers were then sliced into smaller pieces and used to assemble multiple parallel plate cells (Figure 3). A reaction solution consisting of 5 millimolar (mM) substrate **1**, 500 micromolar (μM) tetrabutylammonium hexafluorophosphate (TBA PF_6) electrolyte, and 10 μM rhodium tetraphenylporphyrin iodide (RhTPPI) catalyst in dichloromethane solvent was added to the cell via pipette. The cell was then compressed in a vice and a potential difference applied to the copper mesh contacts. The reaction was allowed to run overnight then stopped. The cell was opened and the reaction solution examined by high pressure liquid chromatography to determine total product conversion and product ratio.

Results and Conclusions:

When using an aluminum oxide dielectric in our parallel plate cell, we found that we could not alter the selectivity in this reaction by applying a potential difference. As can be seen in Figure 4, the product ratio **2:3** remains at about 10:1 for both a 0 volt (V) and a 4.5 V potential. However, when a titanium oxide dielectric was used, we found that the **2:3** ratio was 11.3:1 at 0 V, but fell to 0.7:1 at 4 V. We also observed electric field-induced selectivity changes when using hafnium oxide and tantalum oxide dielectrics. These results are all shown in Figure 4, which displays product ratio **2:3** as a function of voltage applied to the plate cell for each of the four dielectrics used.

These results support our earlier hypothesis that there exists an electric field-induced interaction between a TiO_2 dielectric and rhodium porphyrin catalyst, which can be used to control selectivity in a chemical reaction. This phenomenon is seen with both HfO_2 and Ta_2O_5 dielectrics, but not with an Al_2O_3 dielectric.

Future Work:

This as-yet untapped phenomenon in catalysis has huge potential as a future tool in industrial and academic chemistry, but several challenges remain before it can be effectively exploited. These include elucidating the mechanism of the selectivity change, developing a method to increase the scale of the reaction cell (the experiments in this study were run on a 75 microliter scale), and determining the applicability to industrially relevant chemical syntheses.

Acknowledgements:

Professor Matthew Kanan, Craig Gorin, the Kanan Lab Group, Dr. Michael Deal, the National Nanotechnology Infrastructure Network Research Experience for Undergraduates (NNIN REU) Program.

References:

[1] Gorin, C., Beh, E., Kanan, M.; "An Electric Field-Induced Change In The Selectivity Of A Metal-Oxide-Catalyzed Epoxide Rearrangement"; Journal of the American Chemical Society, 134, p186-189 (2011).

[2] Gorin, C., Beh, E., Kanan, M.; "Interfacial Electric Field Effects on a Carbene Reaction Catalyzed by Rh Porphyrins"; Journal of the American Chemical Society, 135, p 11257-11265 (2013).

Area-Selective Atomic Layer Deposition: New Recipe Development

Tyler Erjavec
Physics, The Ohio State University

NNIN REU Site: Cornell NanoScale Science and Technology Facility, Cornell University, Ithaca, NY
NNIN REU Principal Investigator: Prof. James Engstrom, School of Chemical and Biomolecular Engineering, Cornell University
NNIN REU Mentors: Wenyu Zhang and Rambert Nahm, School of Chemical and Biomolecular Engineering, Cornell University
Contact: tje43@cornell.edu, jre7@cornell.edu, wz89@cornell.edu

Abstract:

Atomic layer deposition (ALD) allows thin films to be deposited layer-by-layer onto a substrate by a sequential flow of gaseous chemical precursors. These precursors interact with the substrate surface via self-limiting reactions and then the cycle can be repeated until the thin film reaches a desired thickness. Area-selective ALD deposits material onto one substrate while leaving another substrate unaffected. This is applicable in device manufacturing. The focus of this project is to develop a recipe to selectively deposit tantalum nitride (TaN_x) on one surface (SiO_2), while limiting the growth on another surface (Cu). We are interested in the thermal TaN_x ALD system, using pentakis(dimethylamino)tantalum (PDMAT) and ammonia (NH_3) as precursors. From previous studies, we know that PDMAT forms strong bonds with the SiO_2 substrate surface in the first half-reaction of the ALD cycle. We decided to add an 'etchant' — dimethylamine, $(CH_3)_2NH$ (DMA) — to the TaN_x ALD recipe to drive the reaction backwards, selectively favoring deposition on SiO_2. We investigated the effect of DMA concentrations, DMA step placement, DMA dose times, and sub-saturation of PDMAT doses.

Introduction:

Tantalum nitride (TaN_x) is used as a diffusion barrier layer [1] in integrated circuits and devices to prevent copper (Cu) diffusion into the surrounding dielectric. It can be deposited via atomic layer deposition (ALD) onto a substrate via sequential flow of gaseous chemical precursors as seen in Figure 1.

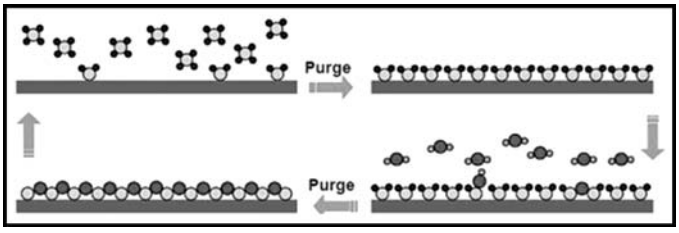

Figure 1: Schematic illustration of the ALD process. Photo Credit: http://gcep.stanford.edu/research/factsheets/atomic_layer_deposition.html

Area-selective ALD deposits material onto one substrate while leaving another substrate unaffected. This has many applications in industrial device manufacturing because it eliminates the need for patterning steps and is potentially more efficient and cost-effective.

Because the Ta precursor used, PDMAT, contains five diethylamido-groups, we have decided to use dimethylamine (DMA) to attempt the reversal of the first half-cycle reaction on Cu.

Experimental Procedure:

In order to develop a selective TaN_x ALD process with the addition of DMA, we decided to test three DMA dose parameters: 1) DMA dose time, 2) DMA dose step-placement, and 3) DMA partial pressure. For each parameter, we deposited 20 cycles of TaN_x on silicon dioxide, SiO_2 (native oxide), and Cu. The nominal sample temperature was 225°C for all depositions. The resulting thin-films were then analyzed using spectroscopic ellipsometry (SE) and wavelength-dispersive x-ray spectroscopy (WDX).

Results and Conclusions:

From spectroscopic ellipsometry (SE), we determined the average growth rate of TaN_x using SiO_2 substrates. SE is model-dependent so results vary depending on which model is used [Ta_2O_5 (because thin films oxidize in air) and Cauchy].

Growth rates of 0.43 Å/cycle (Ta_2O_5 model) and 0.39 Å/cycle (Cauchy model) were obtained, giving an average at approximately 0.4 Å/cycle. This agreed with our expected growth rate of TaN_x on SiO_2. From previous studies, we have found that the Cu substrate is rough and does not form an abrupt interface with the TaN_x layer, preventing reliable SE measurements [2].

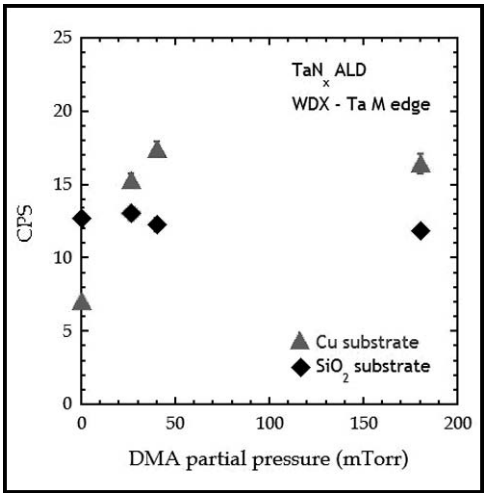

Figure 2: WDX intensities for Ta M edge for TaN_x films deposited on Cu (filled triangles) and SiO_2 (filled diamonds) substrates, plotted against amount of DMA introduced to the system.

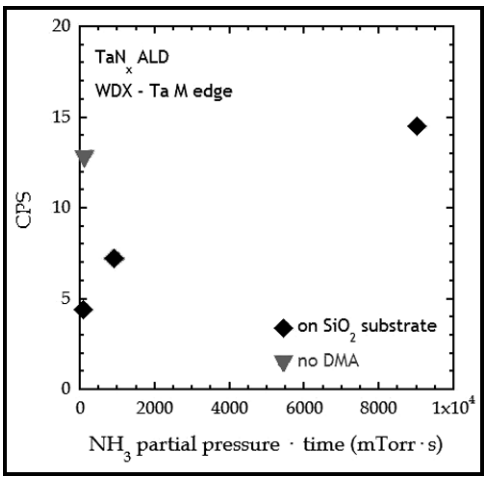

Figure 3: WDX intensities for Ta M edge for TaN_x films deposited on SiO_2 (filled diamonds) substrates, plotted against amount of NH_3 introduced to the system.

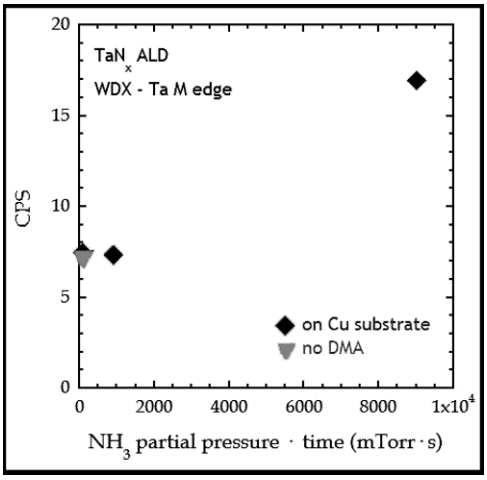

Figure 4: WDX intensities for Ta M edge for TaN_x films deposited on Cu (filled triangles) substrates, plotted against amount of NH_3 introduced to the system.

In Figure 2, we show that DMA partial pressure does not affect TaN_x film growth on SiO_2. On the Cu substrates however, a clear increase in Ta signal is observed with increasing DMA concentration.

We also introduced DMA in the NH_3 dose step (an NH_3|DMA co-exposure) in the hope that the NH_3 would react with the PDMAT on the surface where we wanted it to deposit (SiO_2) while the DMA would act to remove the adsorbed PDMAT from the surface where we did not want TaN_x deposition (Cu). From Figure 3, we see that NH_3|DMA co-exposure exhibited a typical saturation curve as expected. The upside down triangle shows the typical TaN_x recipe, which agrees with the saturated dose of NH_3.

However on the Cu substrates (Figure 4), we see that the TaN_x does not exhibit an expected saturation curve. From this result, we infer that DMA doses do not affect TaN_x on SiO_2 yet increases growth on Cu.

Future Work:

Although manipulating DMA dose placement, step time, and concentration to inhibit TaN_x on Cu — but not SiO_2 — did not affect growth as intended, there are still additional avenues where TaN_x on Cu can be suppressed (ALD temperature, DMA dosage in conjunction with PDMAT sub-saturation doses etc.). Additionally, the stoichiometry of our TaN_x films on SiO_2 and Cu has yet to be determined. We may be depositing more Ta on Cu, but it is likely that many of the ligands from PDMAT were not removed. Future x-ray photoelectron spectroscopy (XPS) measurements will shed some light on this subject.

Acknowledgements:

I would like to thank the National Nanotechnology Infrastructure Network Research Experience for Undergraduates (NNIN REU) Program and the National Science Foundation. I also appreciate guidance, support, and assistance from Wenyu Zhang, James Engstrom, Melanie-Claire Mallison, and the CNF staff. This work made use of the Cornell Center for Materials Research Shared Facilities, which are supported through the NSF MRSEC program (DMR-1120296).

References:

[1] Wang, S. MRS bulletin 19, 30 (1994).

[2] W. Zhang, R.K. Nahm, P.F. Ma, J.R. Engstrom, J. Vac. Sci. Technol. A 31, 061101 (2013).

Poly(3-alkyldithienothiophene): Synthesis, Structure and Optical Properties

Yuki Hamasaki
Applied Chemistry, Kyushu University, Fukuoka, Japan

NNIN iREG Site: NanoTech User Facility, University of Washington, Seattle, WA
NNIN iREG Principal Investigator: Prof. Christine K. Luscombe, Materials Science and Engineering, University of Washington
NNIN iREG Mentor: Dr. Ken Okamoto, Department of Materials Science and Engineering, University of Washington
Contact: y.hamasaki@mail.cstm.kyushu-u.ac.jp, luscombe@uw.edu, keno2@uw.edu

Abstract:

Organic semiconductors that consist of conjugated oligomers or polymers are the subject of considerable current research interest, owing to their fundamental optoelectronic properties and their potential applications for organic photovoltaics. In this context the regioregular alternative copolymer of 3-alkylsulfanylthiophene (AST) and 3-alkylthiophene (AT), *alt*-P3AST-*co*-3AT, has an intriguing structure because the repeating unit can be transformed into 3-alkyldithienothiophen (3ADTT) to serve as a quinoid moiety. The preparation methods of *alt*-P3AST-*co*-3AT are discussed.

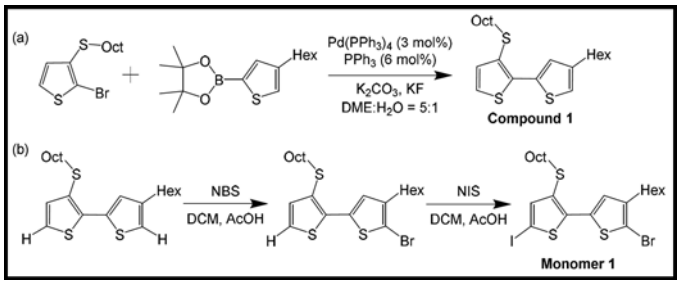

Scheme 1: Monomer synthesis.

Introduction:

Organic electronics is a growing area of research that investigates the properties and applications of conjugated polymers and semiconducting small molecules. Devices made from organic materials have the potential to be flexible, are inexpensive to process, and weigh less than their inorganic counterparts. Organic photovoltaic (OPV) devices are currently under investigation as a low-cost alternative to silicon-based photovoltaic devices. Poly(3-hexylthiophene) (P3HT) is one of the most successful homopolymers due to its semi-crystalline structure, strong light absorption properties, and high charge carrier mobility [1]. However, the short-circuit current density (J_{sc}) and open-circuit voltage (V_{oc}) of P3HT devices are limited due to a wide HOMO-LUMO gap and high HOMO energy level. For these reasons, quinoid polymers are being developed to control the energy levels. Since the quinoid resonance form is lower in energy than the aromatic form, stabilizing the quinoid form will effectively reduce the band gap of related conjugated polymers. According to a theoretical calculation using the Semi-empirical Method, AM1, dehedral angles of regioregular 3-ethylthiophene and 3-thioalkylthiophene, 3-hexyldithienothiophene are 143.8° and 179.5°, 179.7°, respectively.

Here, we report another approach to the design and synthesis of new organic semiconductors for photovoltaics, using the fused thiophene derivative, dithieno[3,2-b:2′,3′-d]thiophene as a building block.

Experimental Procedure:

Synthesis of 5-bromo-4-hexyl-5′-iode-3′-(octylsulfanyl)-2,2′-bithiophene (Monomer 1) via Suzuki coupling method (Scheme 1)

(a) 4-hexyl-3′-(octylsulfanyl)-2,2′-bithiophene (Compound 1). Compound 1 was prepared via Suzuki coupling [2]. In N_2, 2-bromo-3-(octylsulfanyl)thiophene (5 mmol), 4-hexyl-thiophene-2-boronic acid (7 mmol), K_2CO_3 (12.5 mmol, 1.73 g), 10 mL DME and 2 mL distilled water were added to a Schlenk flask. After degas-stirring for 30 minutes, triphenylphosphine (PPh_3) (77.5 mg, 0.3 mmol), $Pd(PPh_3)_4$ (0.173 g, 0.15 mmol) and KF (12.5 mmol, 0.725 g) were added. The mixture was allowed to stir under 90°C (oil bath) overnight. After quenching with NH_4Cl, the reaction mixture was extracted with ethyl acetate. The solvent was evaporated under vacuum. Flash chromatography on silica gel (hexane) gave the Compound 1.

(b) 5-bromo-4-hexyl-5′-iode-3′-(octylsulfanyl)-2,2′-bithiophene (Monomer 1). 4-hexyl-3′-(octylsulfanyl)-2,2′-bithiophene (3.21 mmol, 1.27 g) was added to a flask with 5 mL acetic acid and 5 mL DCM stirring at 0°C. To the flask was added NBS (3.21 mmol, 0.572 g). The solution was brought to room temperature and allowed to stir for one hour before being poured into 50 mL of 10% $Na_2S_2O_3$, and then extracted with diethyl ether. The organic phase was finally dried over anhydrous Na_2SO_4, and evaporated under vacuum to yield a crude oil. Flash chromatography on silica gel (hexanes) gave

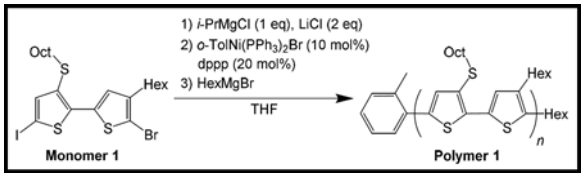

Scheme 2: Polymerization.

the 5-bromo-4-hexyl-3′-(octylsulfanyl)-2,2′-bithiophene. Then, 5-Bromo-4-hexyl-3′-(octylsulfanyl)-2,2′-bithiophene (0.861 mmol, 0.409 g) was added to a flask with 2 mL acetic acid and 2 mL DCM stirring at 0°C. To the flask was added NIS (0.861 mmol, 0.194 g). The solution was brought to room temperature and allowed to stir for 30 minutes before being poured into $Na_2S_2O_3$, and then extracted with diethyl ether. The organic phase was finally dried over anhydrous Na_2SO_4, and evaporated under vacuum to yield a crude oil. Flash chromatography on silica gel (hexanes) gave the Monomer 1.

Initiated Polymerization (Scheme 2). In a procedure adapted from literature [3], Monomer 1 (0.178 g, 0.297 mmol) and 44.5 mg lithium chloride was dissolved in THF (10 mL) and cooled to 0°C with stirring. Then 0.15 mL of a 2.0 M isopropyl magnesium chloride in hexanes was added dropwise over 5 min and stirring continued for 30 minutes. At this point, a solution consisted of 22.3 mg of *cis*-chloro(*o*-tolyl)1,3-bis(diphenylphosphino)propanenickel(II) (10 mol%) and 24.5 mg of diphenylphosphinopropane (dppp) (20 mol%) was added rapidly via syringe. The reaction was allowed to warm to room temperature. The solution was left to polymerize over 10 hours, then quenched with a solution consisted of hexylbromide (0.178 mL, 2 mmol) and magnesium (54.5 mg, 2.2 mmol) in diethyl ether. The reaction mixture was washed by MeOH, acetone, and hexane, in order.

Results and Future Works:

We have succeeded in synthesizing 5-bromo-4-hexyl-5′-iode-3′-(octylsulfanyl)-2,2′-bithiophene, which evaluated by ^{1}H NMR (Figure 1). Polymer 1 showed too complex a NMR spectrum to assign. The next step will be chemical transformation of *ot*-P3OST-*co*-3HT to P3HDTT and measuring the optical properties of synthesized polymer. Moreover, we will fabricate the OPV device consisted of P3HDTT and evaluate their properties.

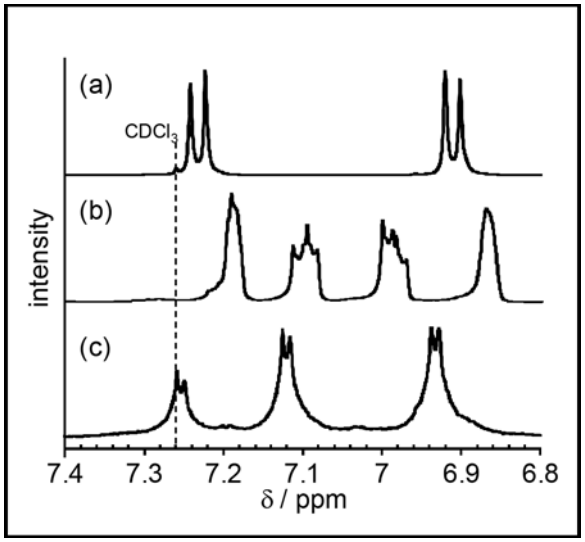

Figure 1: NMR spectra of 2-bromo-3-(octylsulfanyl)thiophene (a), Compound 1 (b), and Monomer 1 (c).

Acknowledgments:

This research was supported by the National Nanotechnology Infrastructure Network (NNIN), the National Science Foundation (NSF) and National Institute for Material Science (NIMS). I would also like to thank the Luscombe Lab for their valuable guidance and assistance, and the NanoTech User Facility (NTUF) at the University of Washington for providing the equipment and training necessary for this project.

References:

[1] Youngkyoo Kim, Jenny Nelson, Donal D. C. Bradley et al., Nature Mater. 2006, 5, 197-203.

[2] Dong, C.-G., T.-P. Liu, and Q.-S. Hu, SYNLETT 2009, 1081-1086.

[3] Hugo A. Bronstein, Christine K. Luscombe, J. Am. Chem. Soc. 2009, 131, 12894-12895.

Synthesis and Characterization of Functional Organic and Supramolecular Nanomaterials

Melinda Jue
Chemical Engineering, University of Texas at Austin

NNIN iREU Site: National Institute for Materials Science (NIMS), Tsukuba, Ibaraki, Japan
NNIN iREU Principal Investigator: Dr. Masayuki Takeuchi, Organic Materials Group, Polymer Materials Unit, NIMS
NNIN iREU Mentor: Dr. Soichiro Ogi, Organic Materials Group, Polymer Materials Unit, National Institute for Materials Science
Contact: melindajue@gmail.com, takeuchi.masayuki@nims.go.jp, ogi.soichiro@nims.go.jp

Abstract:

Artificial photosynthetic systems offer a potential renewable energy source to manage the increasing global energy demand. Organized dye molecules, in particular *J*-type aggregates, exhibit efficient excitation-energy transfer suitable for light-harvesting antennas necessary in artificial photosynthetic systems. We designed and synthesized a porphyrin chromophore (**1S**) so as to self-assemble into a supramolecular polymer with a stable *J*-aggregate mode in solution. Ultraviolet-visible (UV-Vis), infrared (IR), nuclear magnetic resonance (NMR), and circular dichroism (CD) spectroscopic analyses were performed to investigate the aggregation properties.

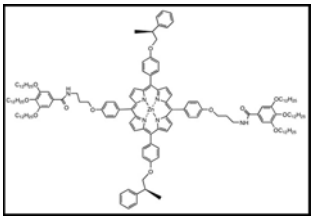

*Figure 1: Chemical structure of **1S**.*

Introduction:

Artificial photosynthesis represents another possibility to harness energy from the sun. In an artificial photosynthetic system, sunlight is absorbed by a light-harvesting antenna before being used to breakdown water into hydrogen and oxygen gas. Ideally a light-harvesting antenna is a chromophore that has a stable *J*-aggregate mode as well useful absorption properties such as broad spectral absorbance and high extinction coefficient [1]. Porphyrin is a conjugated cyclic compound that exhibits self-assembly properties fitting for a potential light-harvesting antenna. It can be synthetically functionalized to form a variety of different chemical structures depending on the application. A natural light-harvesting antenna, chlorophyll, is also a porphyrin derivative [2]. Two aggregation modes, *J*-aggregate and *H*-aggregate, are possible in porphyrin based systems. The *J*-aggregate forms with the porphyrin π systems overlapped partially and the *H*-aggregate is face-to-face stacks of the π systems. Although the H-aggregate is more thermodynamically stable, the *J*-aggregate has desirable light-harvesting properties necessary to transfer energy in artificial photosynthesis. Compound **1S** was designed to form a supramolecular polymer with a stable *J*-aggregate mode in solution.

As seen in Figure 1, **1S** is based on a porphyrin ring with a zinc center. Chiral groups are included to introduce directionality to the aggregate, amide groups to allow for hydrogen bonding, and long alkyl chains to both increase the solubility in nonpolar solvents as well as allow for van der Waals interactions.

Experimental Procedure:

The target molecule was synthesized by a seven step series of reactions starting from pyrrole and ending with **1S**. All compounds were identified with ^{1}H NMR spectroscopy in $CDCl_3$. The aggregation properties of **1S** were characterized with UV-Vis spectroscopy, IR spectroscopy, CD spectroscopy, and atomic force microscopy (AFM). Characterization measurements were taken with solutions of **1S** (10-100 μM) in methylcyclohexane (MCH) at 283-378 K.

Results and Conclusions:

The aggregation properties of **1S** in solution were measured by a combination of spectroscopic techniques. First UV-Vis spectral measurements were conducted to determine the stacking mode of the porphyrin molecules in a MCH solution. At concentration of 50 μM, both Soret and Q bands of the solution were red-shifted in comparison with those of monomeric **1S**, which indicated that the porphyrin molecules overlap in the *J*-aggregate mode. In addition, CD signal was observed with negative maxima at 433 nm, which corresponds to the absorption maximum for Soret band that arises in the UV-Vis spectra upon aggregation. These combined results imply that

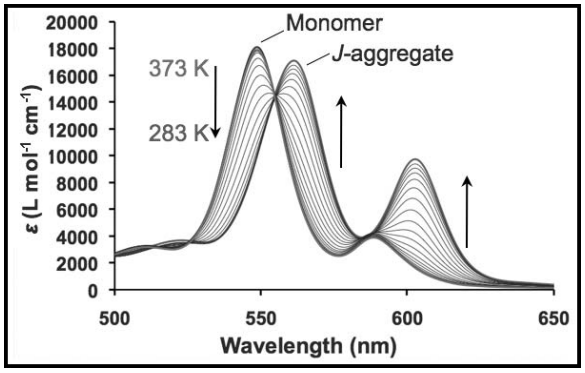

Figure 2: Temperature-dependent UV-Vis spectra of Q band to monitor the formation of J*-aggregate in MCH (*C_T *= 50 μM).*

the chiral groups induce a chiral excitonic coupling between the porphyrin π systems within the *J*-aggregate. IR spectral measurements confirmed both the N-H and C = O stretching vibration peaks were shifted to smaller wavenumbers. These results are indicative of hydrogen bonding between the amide groups of adjacent monomers.

Next the supramolecular polymerization mechanism was investigated with temperature-dependent UV-Vis spectroscopy (Figure 2). As the temperature was decreased from 373 K to 283 K (1 K min^{-1}), a shift of the Q band was induced with a sigmoidal transition that is characteristic of the isodesmic mechanism. This mechanism assumes that each species of aggregation (monomer, dimer, trimer, etc.) are formed with a same equilibrium constant (K_e).

Based on the isodesmic model, the equilibrium constant can be described using Equation 1, where the left side is a fraction of monomeric **1S**, and C_T is an initial concentration of **1S** [3]. The aggregation process was well fitted by an isodesmic analysis, which yielded equilibrium constants at various temperatures. A van't Hoff plot based on these values showed a linear relationship, from which the standard enthalpy change ($\Delta H°$) and entropy change ($\Delta S°$) were determined to be -88 kJ mol^{-1} and -193 J mol-1 K^{-1}, respectively.

$$\frac{M}{C_T} = \frac{2C_TK_e + 1 - \sqrt{4C_TK_e + 1}}{2(C_TK_e)^2}$$

Equation 1: Isodesmic model for determining equilibrium constant.

Furthermore, the aggregation shape was examined with AFM (Figure 3). The average aggregation height is 2 nm while the minimum distance across **1S** varies from 2.5-2.9 nm based on simulations. From this information, the aggregates lay approximately 50° to the surface and not perpendicularly. This stacking height further indicates that *J*-aggregates are formed in solution as well as on the substrate.

In conclusion, we successfully synthesized **1S** and characterdized its aggregation behavior. From the results of various spectroscopic analyses, we revealed that **1S** could form a stable *J*-aggregate with the twisted absorption transition dipoles through π–π stacking and hydrogen bonding in MCH. The aggregation mechanism was well fitted by an isodesmic model so that the equilibrium constant and the thermodynamic properties were determined. Compound **1S** exhibits properties that are beneficial to the synthesis of a light-harvesting antenna.

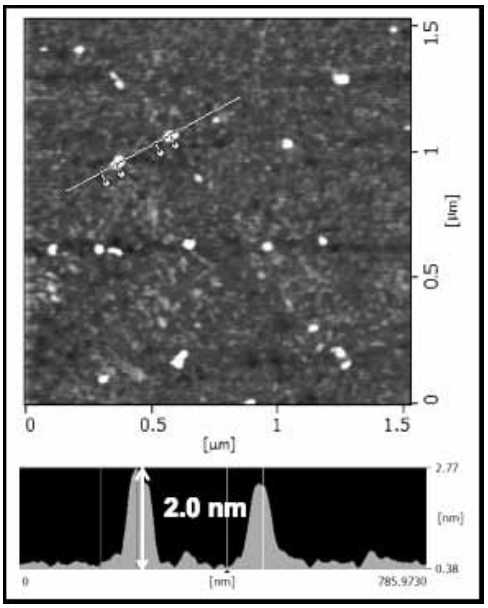

Figure 3: AFM height image of the J*-aggregate spin-coated onto a silicon wafer from a MCH solution.*

Acknowledgments:

Thank you to Dr. Soichiro Ogi, Dr. Kazunori Sugiyasu, Dr. Masayuki Takeuchi, the National Institute for Materials Science, the National Nanotechnology Infrastructure Network International Research Experience for Undergraduates (NNIN iREU) Program, and the National Science Foundation for making this research possible.

References:

[1] Frishmann, P. D., et al., Powering the future of molecular artificial photosynthesis with light-harvesting metallosupramolecular dye assemblies, Chem. Soc. Rev., 2013, 42, 1847-1870.

[2] Wurthner, F., et al., J-aggregates: From serendipitous discovery to supramolecular engineering of functional dye materials, Angew. Chem. Int. Ed., 2011, 50, 3376-3410.

[3] Martin, R. B., Comparisons of indefinite self-association models, Chem. Rev., 1996, 96,3043-3064.

Crumpled Graphene Oxide Nanostructures for Advanced Water Treatment Technologies

Christine Le
Biochemistry, Brown University

NNIN REU Site: Nano Research Facility, Washington University in St. Louis, St. Louis, MO
NNIN REU Principal Investigator: Dr. John Fortner, Energy, Environmental, and Chemical Engr., Washington University in St. Louis
NNIN REU Mentor: Yi Jiang, Energy, Environmental, and Chemical Engineering, Washington University in St. Louis
Contact: christine_le@brown.edu, jfortner@seas.wustl.edu, jiang.y@wustl.edu

Abstract:

The global water crisis calls for water treatment technological advancements, which, based on the state of the art, will be increasingly underpinned by engineering/application of nanoscale materials. Our project aimed to develop an efficient aerosol-based technique to synthesize crumpled graphene oxide (CGO) nanocomposites for enhanced water purification applications. Specifically, we aimed to synthesize and characterize two types of CGO nanocomposites: CGO-TiO_2 (as a high-performance photocatalyst for pollutant degradation) and CGO-magnetite (as a monomeric self-assembling component of a robust and magnetically manipulatable thin-film membrane). We also intended to examine CGO nanocomposites' water-stability under different water chemistries (such as pH). Scanning electron microscopy (SEM) and transmission electron microscopy (TEM) were utilized for size and morphology measurement while electrophoretic light scattering (ELS) and dynamic light scattering (DLS) were used to test zeta potential and nanoparticle size, respectively. Our results indicate an inverse relationship between pH and mean nanoparticle size, and solutions with pH > 3.0 enable CGO stability (zeta potential < -30 mV).

Introduction:

Currently, there are over three million deaths annually, resulting from water-, sanitation-, and hygiene-related diseases [1]. According to the World Water Council, 3.9 billion people are predicted to live with deficient and unsanitary water supply by 2030 [2].

Thus, our project aimed to construct a water treatment membrane using a thin film of CGO-based nanocomposites consisting of both encapsulated photocatalytic materials like TiO_2, which enables enhanced photo-reactive (UVA irradiation) activity for organic pollutant degradation, and adequate amounts of monomeric, nanoscale magnetite components, allowing for magnetic manipulation of nanocomposites in water. CGO provides the membrane with sufficient accessible surface area for water permeability and increased pollutant adsorption.

Two-dimensional graphene oxide has been extensively researched previously because of its unique nanosheet morphology, extreme specific surface area (~ 2650 m^2/g) and broad chemical functionalization possibilities. However, restacking issues caused by van der Waals attraction between the sheets significantly reduces its surface area, thereby limiting its applications. Fortunately, a new field has opened up with the discovery of three-dimensional CGO [3]. Its properties, which include a crumpled ball-like morphology, high free volume, and aqueous stability, make it an ideal candidate for various applications, including water treatment.

Experimental Procedure:

Graphene oxide was synthesized using a modified Hummers method [4]; TiO_2 (Degussa Aerodisp 740X) and magnetite (Fe_3O_4, Sigma Aldrich) were used. A furnace aerosol reactor was used to synthesize CGO through an aerosolization process. First, a Collison nebulizer atomized a GO-TiO_2 precursor into fine droplets; and the droplets were delivered by N_2 into the furnace. Crumpling of GO and encapsulation of TiO_2 was induced by capillary compression caused by rapid evaporation of the aerosol droplets in the furnace (400°C). Finally, CGO nanocomposites were collected at the downstream of the reactor. SEM (NOVA NanoSEM 230) and TEM (Tecnai TM Spirit) were used to determine the size and morphology of the CGO. Zeta potential and aqueous nanoparticle size distribution were measured by ELS and DLS, respectively (Malvern Zetasizer Nano ZS).

Results and Discussion:

GO crumpled and TiO_2 successfully became encapsulated, as evidenced from the SEM (Figure 1) and TEM (Figure 2) images. The SEM images illustrated the nanocomposites' crumpled ball-like morphology, while the TEM images confirm TiO_2 encapsulation and nanoparticles with a size range of 250-350 nm. The CGO nanocomposites had a quasi-spherical morphology resembling a crumpled piece of notebook paper, considerably smooth surfaces, and black color. The color results from GO reduction.

Figure 3 displays ELS results showing the relationship between pH and zeta potential of the aqueous GO-TiO_2 solution. Zeta

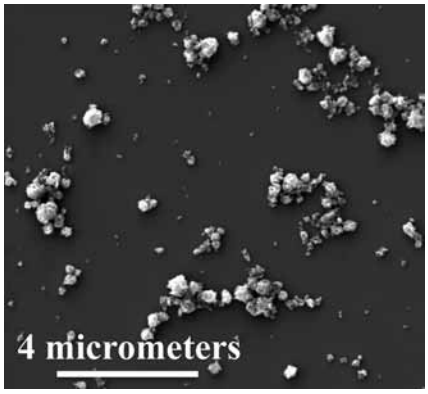

Figure 1: The SEM image demonstrates CGO's crumpled ball morphology.

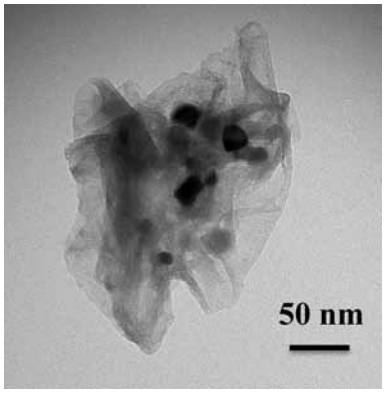

Figure 2: The TEM image denotes TiO_2 encapsulation.

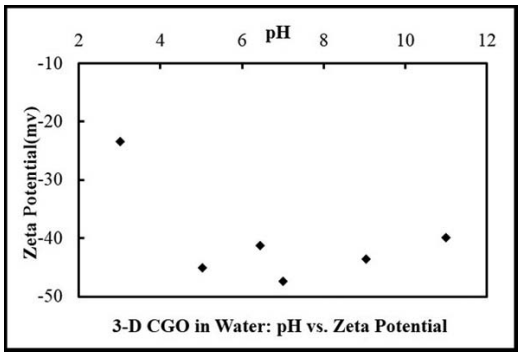

Figure 3: The relationship between pH and zeta-potential of GO-TiO_2 solution.

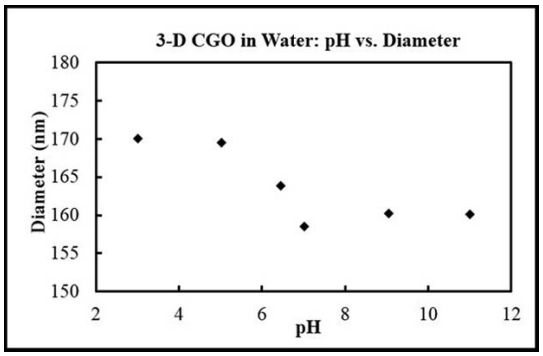

Figure 4: The relationship between pH and nanoparticle size of GO-TiO_2 solution. As pH increases, NP size decreases.

potential, reflecting a nanoparticle's surface charge, indicates the degree of its tendency to resist aggregation and therefore its stability in solution. The data suggested that solutions with pH > 3 yield stable CGO (< -30 mV).

A general inverse relationship was also observed between pH and nanoparticle size (Figure 4). Higher pH values (more basic) imply large OH-concentrations, which enable more negative CGO surface charges. The repulsive electrostatic forces increased between nanoparticles, leading to less aggregation and smaller nanoparticles.

Understanding the interrelationship between pH, nanoparticle size, and zeta potential will facilitate tailoring of CGO behavior according to the acidic conditions of aqueous suspensions for optimized water purification.

Future Work:

Doping TiO_2 has attracted research interest because it narrows TiO_2's band gap, allowing it to activate under sunlight exposure, hence minimizing energy costs. Doping is when impurities are added to semiconductor crystals to tune their conductivity and other characteristics. We will experiment with various dopants/dopant combinations to measure their efficacy in further enhancing TiO_2's photocatalytic properties. A porous, reactive, thin-film membrane will be assembled using the fabricated CGO and a polyvinylidene difluoride support membrane.

Membrane performance will be tested using ultraviolet-visible light spectroscopy and methyl orange will be employed as a model pollutant.

Acknowledgments:

I would like to thank the National Nanotechnology Infrastructure Network Research Experience for Undergraduates Program and National Science Foundation for their generous support, as well as Dr. John Fortner, Yi Jiang, Fortner lab, Dr. Wei-Ning Wang, the Nano Research Facility, Nathan Reed, Dee Stewart, Howard Wynder, Kate Nelson, and Lijie Zhang for their encouragement and guidance.

References:

[1] WHO/UNICEF, Progress on Drinking Water and Sanitation: 2012 Update. 2012, WHO/UNICEF: Geneva/New York.

[2] Urban Urgency, Water Caucus Summary, World Water Council (WWC), Marseille, France, 2007.

[3] Wang, W.-N., Y. Jiang, and P. Biswas, Evaporation-Induced Crumpling of Graphene Oxide Nanosheets in Aerosolized Droplets: Confinement Force Relationship. J. of Physical Chemistry Letts, 2012. 3(21): p. 3228-3233.

[4] W.S. Hummers and R.E. Offeman, Preparation of Graphitic Oxide. Journal of the American Chemical Society, 1958. 80(6):1339-1339.

Direct Nano Patterning of Anisotropic Conjugated Polymer

Azusa Miyagawa
Materials Science, Japan Advanced Institute of Science and Technology, Ishikawa Prefecture, Japan

NNIN iREG Site: Lurie Nanofabrication Facility, University of Michigan, Ann Arbor, MI
NNIN iREG Principal Investigator: Dr. Jinsang Kim, Materials Science and Engineering, University of Michigan
NNIN iREG Mentors: Dr. Pilar Herrera-Fierro, Lurie Nanofabrication Facility, University of Michigan;
Kyeongwoon Chung, Materials Science and Engineering, University of Michigan
Contact: s1340015@jaist.ac.jp, jinsang@umich.edu, pilarhf@umich.edu, kychung@umich.edu

Abstract:

Conjugated polymers with a one-dimensional p-orbital overlap exhibit optoelectronic anisotropy. Their unique anisotropic properties can be fully realized in device applications only when the conjugated chains are aligned. To align chains, we directly drew conjugated polymer lines via dip pen nanolithography (DPN) using a NanoInk DPN 5000. As the first step, poly(3-hexylthiophene) was used as a polymeric material and patterned lines on a gold (Au) surface, changing the solution concentration and writing speed. The line quality was evaluated by fluorescence microscope and atomic force microscope. Our results indicated that solution concentration was not important, but writing speed was critical for writing continuous lines. There are more factors to be considered to write fine lines. However we also revealed that nanoscale lines can be written by DPN technique.

Introduction:

Conjugated polymers (CPs) are active materials for various optoelectronic applications, such as organic solar cells, thin film transistors and light-emitting diodes. Their highly anisotropic optical and electronic properties are owing to the one-dimensional p-orbital overlap along the conjugated polymer backbone. However, these properties of conjugated polymer cannot be fully realized in device applications unless CPs are molecularly and macroscopically assembled and aligned with a well-defined structure. In reality, the directed assembly and particularly macroscopic alignment of CPs is a challenging task, because CPs do not have good self-organization owing to their non-planar structure in solution.

In our previous work, we could obtain well-defined conjugated polymer films by setting of molecular-design rules for improving the directional alignment of CPs under the application of shear stress [1]. In this study, to further improve the CPs alignment, the dip pen nanolithography (DPN) technique was used to make well-aligned CP lines in nanoscale, which is known to be potentially capable of patterning in the nanometer range [2-4]. The DPN process uses a scanning probe tip (the "pen") to directly deposit a material ("ink") with nanoscale onto a substrate. The influence of writing speed and solution concentration on the line continuity was investigated.

Experimental Procedure:

The polymeric material used in this study was poly (3-hexyl-thiophene) (P3HT) purchased from Rieke Metals. P3HT was dissolved in a mixture of o-dichlorobenzene and 1.8-octanedithiol (10:1) and filtered through a 0.45 μm PTFE filter before use. Solution concentrations were 2.5 and 10 g/l. Silicon wafers with a gold (Au) top layer were used. Au substrates were cut into pieces of 1 cm × 1 cm and cleaned by immersion in acetone. The substrates were treated with oxygen plasma.

DPN was carried out using a DPN 5000 (NanoInk, Inc.) in an atmosphere control chamber. Lithography was performed at a temperature of 25°C and 50% relative humidity. The writing speed were 1.0 and 0.001 mm/s. Silicon nitride single pens (Type A, NanoInk, Inc.) were used. The ink was filled in an Inkwell (IWL-0031-01, NanoInk, Inc.). Image analyses were done with the Olympus BX-51 fluorescence microscope (FM) and Nano Man atomic force microscope (AFM).

Results and Conclusions:

Fluorescent Microscopy. Figure 1 shows the FM image of the line written with the ink of 2.5 g/l concentration and the writing speed of 0.001 mm/s. Changing concentrations did not show any noticeable changes in the line continuity. However, continuous lines were not generated via a writing speed of 1.0 mm/s, even though that writing speed was critical for line quality. Furthermore, it was found that lines could be written more than 1000 μm on a one-time ink loading.

Atomic Force Microscopy. The AFM topography image of generated lines with the ink of 10 g/l concentration and the writing speed of 0.001 mm/s is shown in Figure 2. Changing concentration also does not show a difference even in AFM images, indicating that the solution concentration does not affect the line continuity. The AFM image of the cross section reveals that the generated line width and thickness was 0.8 μm and 20 nm, respectively (Figure 3).

Comparing direct writing processes, whereas inkjet printing is limited to feature sizes of some tens of microns [5], generated lines in this study are the nanometer range. However, even written in the same condition, continuous lines are not obtained constantly. This indicates that there are more parameters to be considered to write continuous lines. For instance, ink amount of the probe [3], probe conditions [4], humidity [2], writing force and surface conditions are also important to writing patterns and we have to consider them.

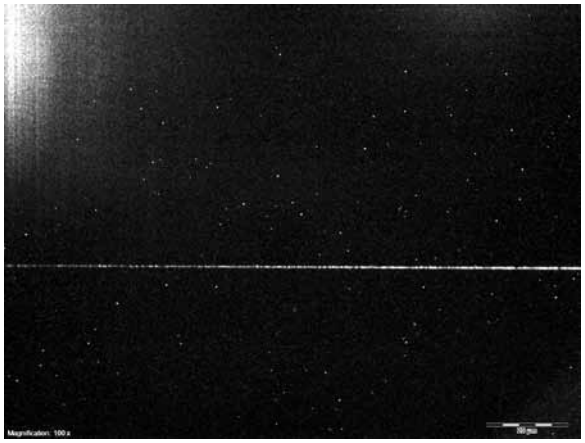

Figure 1: The FM image of P3HT line written with 2.5 g/l concentration ink.

Future Work:

The most important is to write continuous lines constantly. We need to write lines with changing other properties such as ink amount, writing force and humidity.

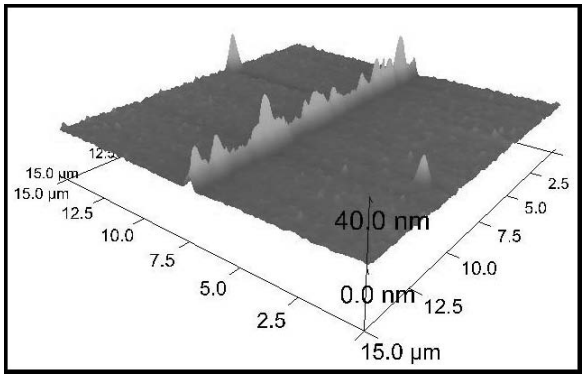

Figure 2: The AFM image of P3HT line written with 10 g/l concentrations ink.

Acknowledgements:

I would like to thank the National Nanotechnology Infrastructure Network International Research Experience for Graduates (NNIN iREG) Program, the National Science Foundation, Nanotechnology Platform, Japan, the Lurie Nanofabrication Facility and staff, Dr. Jingsan Kim, Dr. Pilar Herrera-Fierro, and Mr. Kyeongwoon Chung.

References:

[1] Kim, B., Jeong, E., Chung, J. W., Seo, S., Koo, B., Kim, J. "A molecular design principle of lyotropic liquid-crystalline conjugated polymers with directed alignment capability for plastic electronics." Nature Mater. 12, 659 (2013).

[2] Wang, H. T., Nafday, O. A., Haaheim, J. R., Tecaarwerk, E., Amro, N. A., Sanedrin, R. G., Chang, C. Y., Ren, F., Pearton, S. J. Toward conductive traces: Dip Pen Nanolithography of silver nanoparticle-based inks. Appl. Phys. Lett. 93, 143105 (2008).

[3] Kramer, M. A., Ivanisevic, A. Parallel dip-pen nanolithography using spore- and colloid- terminated cantilevers. Small 8, 3791 (2012).

[4] Lenhert, S., Sun, P., Wang, Y., Fuchs, H., Mirkin, A. Massively parallel dip-pen nanolithography of heterogeneous supported phospholipid multilayer patterns. Small 3, 71 (2007).

[5] Calvert, P. Inkjet printing for materials and devices. Chem. Mater. 13, 3299 (2001).

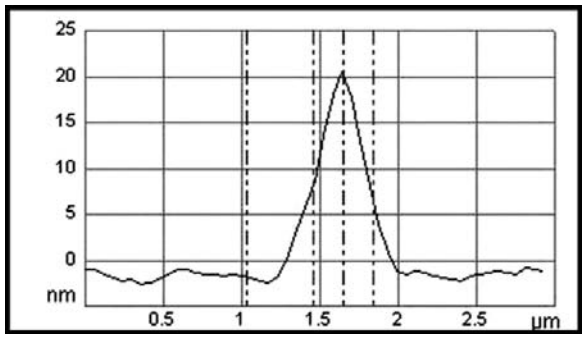

Figure 3: The AFM image of the cross section for Figure 2.

Synthesis and Covalent Attachment of $\{M_4\}$ Polynuclear Metallic Complexes to Oxidized Carbon Nanotubes

Christopher A. Nakamoto
Chemistry, Beloit College

NNIN iREU Site: Institut Für Bio- Und Nanosysteme (IBN), Forschungszentrum, Jülich, Germany
NNIN iREU Principal Investigator: Dr. Carola Meyer, PGI-6, Jülich Forschungszentrum
NNIN iREU Mentor: Dr. Claire Besson, PGI-6, Jülich Forschungszentrum
Contact: nakamoto.c60@gmail.com, c.meyer@fz-juelich.de, c.besson@fz-juelich.de

Introduction:

Carbon nanotubes (CNTs) are one-dimensional conductors with excellent spin transport properties that can be modified by chemical functionalization. This makes them an extremely interesting material for spintronic applications. For example, grafting single molecule magnets to CNTs through π–π interactions produces magnetoresistance [1]. Such dispersion forces are relatively weak, though, resulting in poor adhesion or orientation.

In contrast, covalent bonding offers stronger, better-oriented functionalization of CNTs and has been demonstrated with tetramaganese(II) $\{Mn_4\}$ complexes and oxidized CNTs; $\{Mn_4\}$ represents the general formula $[Mn_4L_2(CH_3COO)_4]$ (H_2L=2,6-bis(1-(2-hydroxyphenyl)iminoethyl)pyridine) [2]. The $\{Mn_4\}$ consists of a Mn_4O_4 cubane core held in place by rigid ligands and capped by exchangeable acetate ligands [3]. The exchange of these carboxylate ligands has little effect on the overall structure and magnetic behavior of $\{Mn_4\}$. This is ideal for a ligand exchange route of covalent functionalization. In the case of oxidized CNTs, carboxylate functionalities on the CNTs exchange with acetates in $\{Mn_4\}$ to directly bind to the metal nuclei of $\{Mn_4\}$.

In this report the versatility of ligand exchange functionalization is demonstrated with oxidized CNTs and two newly synthesized $\{M_4\}$ (M = Co, Zn) complexes with chemical structures similar to $\{Mn_4\}$. The effects of functionalization on resistivity at room temperature are additionally explored.

Experimental Procedure:

Co_4[2,6-bis(1-(2-hydroxyphenyl)iminoethyl)pyridine]$_2$[acetate]$_4$. A mixture of 2,6-diacetylpyridine (400.3 mg, 2.45 mmol), 2-aminophenol (536.4mg, 4.91 mmol), and $Co(CH_3CO_2)_2 \cdot 4H_2O$ (1,2298 g, 4.94 mmol) in methanol (5 ml) was refluxed for 3.5 hours under argon (Ar) to obtain a dark-orange solution. After cooling, degassed diethyl ether (20 ml) was transferred to the solution by cannulation to produce dark-red crystals and orange microcrystalline powder. Recrystallization from ethanol top-layered with pentane afforded the product as red crystals (180.6 mg, 74.2% yield).

Zn_4[2,6-bis(1-(2-hydroxyphenyl)iminoethyl)pyridine]$_2$[acetate]$_4$. A mixture of 2,6-diacetylpyridine (400.1 mg, 2.45 mmol), 2-aminophenol (536.2mg, 4.91 mmol), and $Zn(CH_3CO_2)_2 \cdot 2H_2O$ (1.0853 g, 4.94 mmol) in methanol (20 ml) was refluxed for two hours in air to obtain a dark-orange solution. After cooling, diethyl ether (100 ml) was transferred to the solution slowly to produce needle-like, orange crystals and light-orange powder. Recrystallization by slow evaporation of chloroform afforded orange crystals.

Mn_4[2,6-bis(1-(2-hydroxyphenyl)iminoethyl)pyridine]$_2$[acetate]$_4$. $\{Mn_4\}$ was synthesized following the procedure outlined by Kampert et al. [3].

$\{M_4\}$ Characterization. The $\{M_4\}$ complexes were characterized by IR, Raman, UV-Vis spectroscopy, single crystal XRD, and cyclic voltammetry. The $\{Zn_4\}$ was further characterized by ^1H and ^{13}C NMR.

Preparation of CNT Networks. A catalyst solution of AEROXIDE® Alumina (24.7 mg, 242 μmol), $Fe(NO_3) \cdot 9H_2O$ (41.4 mg, 171 μmol), and bis(acetylacetonato)-dioxomolybdenum(VI) (8.6 mg, 26 μmol) in methanol (30 ml) was prepared by 10 min of sonication. One by one centimeter square pieces of <100> Si with an insulating layer of SiO_2 were treated with a few drops of catalyst solution and dried under a N_2 stream, followed by heating at 120°C to remove solvent. Samples were placed in a quartz tube furnace and heated under Ar to 850°C. Once at 850°C, Ar flow was stopped and a mixture of 520 sccm CH_4 and 700 sccm H_2 was passed over the samples for 10 min followed by cooling under Ar. Formation of carboxylate functionalities on the CNTs occurred by oxidation in air at 450°C for 8 min.

CNT Network Characterization. CNT networks were characterized by atomic force microscopy (AFM) to ensure adequate coverage and growth density. Electronically, oxidized CNT networks were tested before and after functionalization using a two-terminal setup and e-beam evaporated Pt contacts.

CNT Network Functionalization. Oxidized CNT networks were placed in acetonitrile solutions containing 2.5 mg/ml of $\{Co_4\}$, $\{Zn_4\}$, or $\{Mn_4\}$ and left to sit for one week with a

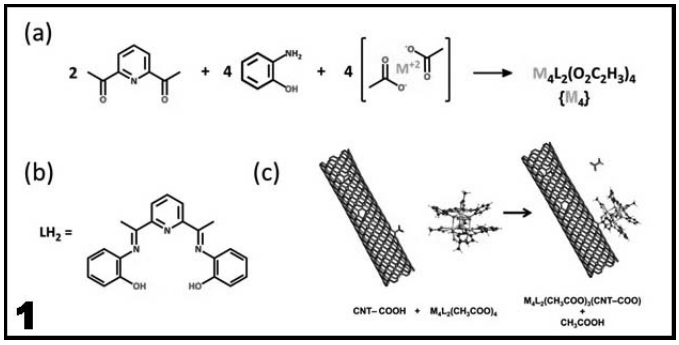

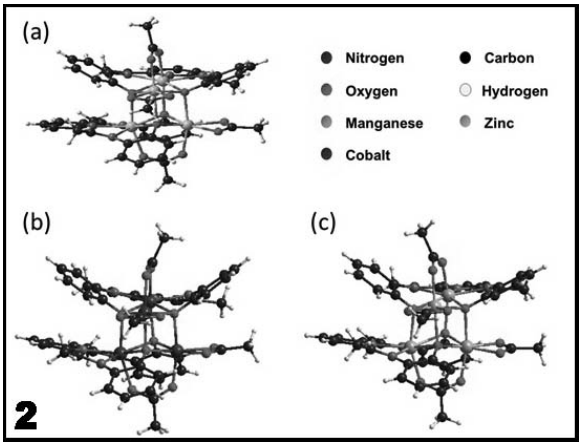

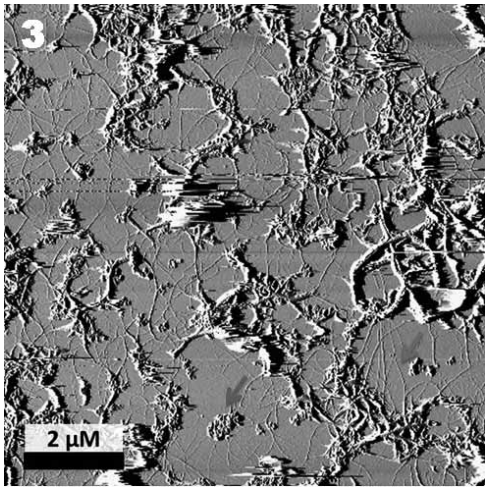

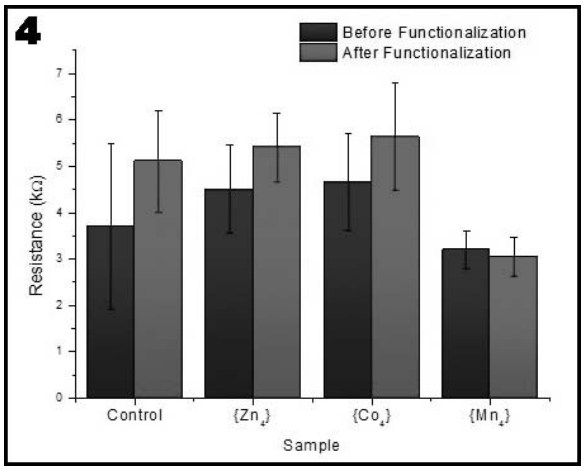

control in pure acetonitrile. To rinse the samples thoroughly, the samples were soaked in acetonitrile for four days followed by three more days in fresh acetonitrile.

Results and Discussion:

{Co_4} and {Zn_4} Synthesis. Figure 1a shows a reaction scheme for the synthesis of {Mn_4}, {Co_4}, and {Zn_4}. The resulting crystal structures obtained by x-ray crystallography, shown in Figure 2, demonstrate the syntheses were successful despite using metals with different preferred coordination geometries. (See a full-color version of Figure 2 on the inside cover.) The {M_4} species are extremely similar in structure consisting of a metal-oxide cubane core held in place by the ligand shown in Figure 1b. Similarities in the positioning of acetate ligands imply ligand exchange with CNTs is possible for all three shown schematically in Figure 1c.

CNT Network Characterization. AFM of the CNT networks showed dense CNT growth and good substrate coverage, shown in Figure 3. Al_2O_3 supported catalyst particles can also be observed. Electrical characterization of the CNT networks before and after functionalization with {M_4} indicated no change in resistance within a 95% confidence interval as seen in Figure 4, although there is a trend of increased resistance with functionalization.

Conclusions:

Two new {M_4} complexes with a similar structure to {Mn_4} were synthesized using Zn^{+2} and Co^{+2}. All three {M_4} complexes were reacted with oxidized CNT networks and were found to have a statistically insignificant effect on CNT networks resistances at room temperature.

References:

[1] Urdampilleta, M., Klyatskaya, S., Cleuziou, J.P., Ruben, M., Wernsdorfer, W. Nat. Mater. 2011, 10(7), 502-506.

[2] Meyer, C., Besson, C., Frielinghaus, R., Saelhoff, A.-K., Flötotto, H., Houben, L., Kögerler P., Schneider, C. M. Phys. Status Solidi B. 2012 249(12), 2412-2415.

[3] Kampert, E., Janssen, F.F.B.J., Boukhvalov, D.W., Russcher, J.C., Smits, J.M.M; Gelder, R., Bruin, B., Christianen, P.C.M., Zeitler, U., Katsnelson, M.I., Maan, J.C., Rowan, A.E. Inorg. Chem. 2009, 48, 11903-11908.

Effects of Hydrophilic Membrane Modifications and Natural Organic Matter Fouling on Reverse Osmosis Membrane Performance

Justin Nauman
Chemical Engineering, Purdue University

NNIN REU Site: Nano Research Facility, Washington University in St. Louis, St. Louis, MO
NNIN REU Principal Investigator: Dr. Young-Shin Jun, Energy, Environmental, and Chemical Engr., Washington University in St. Louis
NNIN REU Mentor: Ms. Jessica Ray, Energy, Environmental, and Chemical Engr., Washington University in St. Louis
Contact: nauman@purdue.edu, ysjun@seas.wustl.edu, jessica.ray@go.wustl.edu

Abstract:

Reverse osmosis diffusion processes offer an effective method for filtering brackish and sea waters. Thin-film composite (TFC) membranes function as the filter in these systems. However, the main drawback to using the TFC membranes is their susceptibility to fouling by hydrophobic natural organic matter (NOM) and various inorganic salts commonly found in brackish waters. One proposed method of mitigating this problem is to modify the polyamide active layer of the TFC membrane to be more hydrophilic using polyethylene glycol (PEG). The focus of the project is to determine the effect of hydrophilic PEG grafting on membrane performance in the presence of NOM and model brackish water constituents. Using a tabletop reverse osmosis setup, feed stream conditions containing NOM and/or aqueous salts were tested for both grafted and unmodified membranes. Analysis of the permeate stream indicated that PEG-grafted membranes reduced permeate flux but also increased the ion rejection in most systems.

Introduction:

The desalination of brackish water and seawater is employed to provide fresh water to people around the world. A common method of desalinating water is reverse osmosis (RO), where an applied pressure is used to overcome the osmotic pressure through a semipermeable membrane. A feed stream often containing inorganic salts and NOM (which are generally hydrophobic) is fed to the system, with permeate, or filtered, and concentrate streams leaving the system [1]. However, the TFC membranes, shown in Figure 1, used during the process are often fouled by the deposition and clogging of pores caused by the NOM and salts present in the feed stream. This reduction in efficiency leads to less effective filtration and more frequent membrane cleaning/replacement [2].

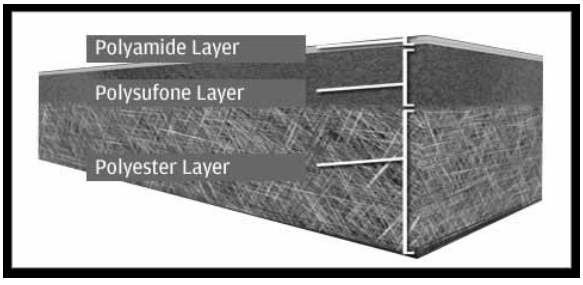

Figure 1: TFC membrane displaying the three layers including the top polyamide active layer [2].

One proposed method of mitigating this problem is to modify the top polyamide layer of the TFC membrane to be more hydrophilic and resistant to fouling. PEG has been determined to be a suitable candidate for this process because it is a flexible, water-soluble polymer with a hydrophilic head [3].

Experimental Procedure:

Membranes were tested using a reverse osmosis benchtop setup to determine their fouling characteristics in different feed solutions. Half of these membranes were grafted with PEG using a cross-linker solution of ethylene glycol dimethacrylate and potassium disulfate and potassium persulfate initiators. The membranes were placed in the system depicted in Figure 2. The various feed solutions were placed in the plastic tub and

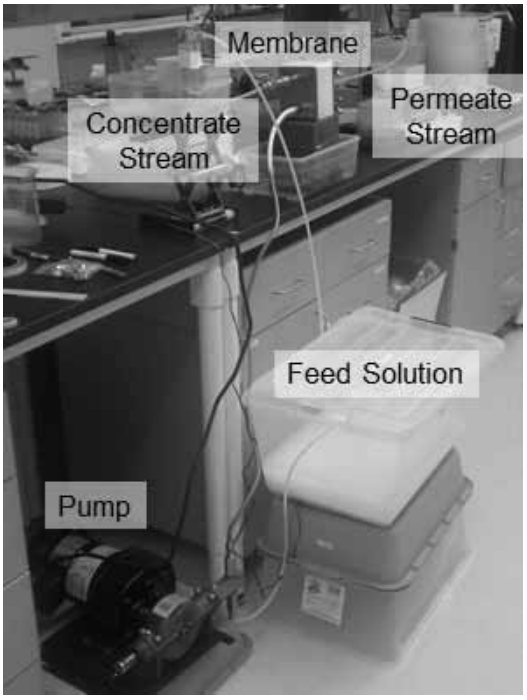

Figure 2: Reverse osmosis benchtop setup used for testing.

each system was left to run for four hours. The feed streams all contained one molar sodium chloride and at least one added potential fouling agent. For our potential foulants we used humic acid as the NOM and calcite ($CaCO_3$) and gypsum ($CaSO_4$) as our salts, two common foulants found in brackish waters. An autosampler collected a sample of the permeate stream every three minutes during the experiment. After each system finished running, we measured the calcium and chlorine ion concentrations in the permeate stream using ion selective electrodes. Permeate flux was also calculated using the collected volume in each test tube. The NOM concentration was measured using a Total Organic Carbon Analyzer. We then took a sample from each used membrane and analyzed the fouling morphology using scanning electron microscopy (SEM).

Results and Conclusions:

From the SEM images gathered, the calcite was found to form a consistent rhombohedra aggregate on the surface of the membrane. The gypsum formed more irregular rod and sheet-like structures. From the ion concentration data, we found that PEG-grafted membranes had an increased ion rejection (calcium and chloride) in calcite forming systems, but a decreased ion rejection in gypsum forming systems, as shown in Figure 3. When systems containing just the calcium salt and systems containing both a calcium salt and humic acid were tested, the PEG-grafted membranes in the gypsum (Ca^{2+} - SO_4^{2-}) systems also showed more overall fouling than the unmodified systems, even at a lower saturation index. In addition, PEG-grafted membranes did also reject more NOM than their unmodified counterparts as you can see in Figure 4. Interestingly, the PEG-grafted gypsum system did not reject the humic acid as well as the PEG-grafted calcite system or the PEG-grafted system with only humic acid, but it did perform better than the unmodified gypsum system. However, PEG-grafted membranes also resulted in a lower permeate flux amounting at about a 65% decrease in systems not containing NOM and roughly a 33% decrease in systems containing NOM. Cost analysis would have to be performed to determine if the PEG modification to the TFC membranes would be economically beneficial because the decrease in flux could potentially outweigh the benefit of increased NOM and ion rejection (except in gypsum systems).

Future Work:

The next step would be to replicate the reverse osmosis test. Ideally, more systems would also be tested using other inorganic salts and NOM commonly found in brackish waters, such as $MgSO_4$ and $MgCO_3$. Another important aspect to further investigate is the driving force of the inverse effects of fouling in Gypsum systems.

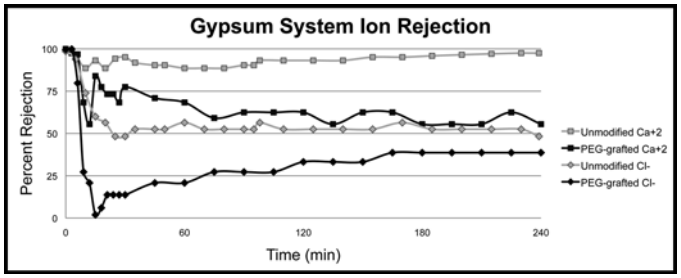

Figure 3: Graph modeling gypsum system ion rejection.

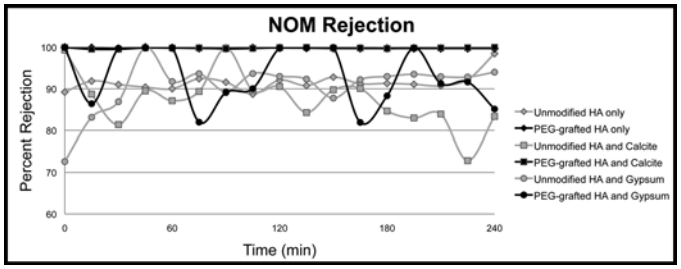

Figure 4: Graph modeling NOM rejection.

Acknowledgments:

I would like to thank Dr. Young-Shin Jun, Ms. Jessica Ray, and everyone at the Environmental Nanochemistry Lab for their guidance and support. I would also like to acknowledge the National Nanotechnology Infrastructure Network Research Experience for Undergraduates Progam and the National Science Foundation for giving me this exceptional opportunity and experience.

References:

[1] Greenlee, et al., Reverse osmosis desalination: Water sources, technology, and today's challenges. Water Research, Volume 43, Issue 9, Pages 2317-2348, May 2009.

[2] Elimelech, M., and Phillip, W. A. The future of seawater desalination: Energy, technology, and the environment. Science, 333 (6043), 712-717, 2011.

[3] Tiraferri, et al., Superhydrophilic Thin-Film Composite Forward Osmosis Membranes for Organic Fouling Control: Fouling Behavior and Antifouling Mechanisms. Environmental Science and Technology, 46 (20), 11135-11144, 2012.

Controlled Self-Assembly of Metallated and Non-Metallated Peptidic Arrays

Geoffrey Vrla
Chemistry, Middlebury College

NNIN iREU Site: National Institute for Materials Science (NIMS), Tsukuba, Ibaraki, Japan
NNIN iREU Principal Investigator and Mentor: Dr. Kentaro Tashiro,
Reticular Materials Group, National Institute for Materials Science
Contact: gvrla@middlebury.edu, tashiro.kentaro@nims.go.jp

Abstract:

Peptide-based compounds are desirable targets for the development of novel nano-materials due to their propensity to form self-assembled, supramolecular architectures. Chemical modification of self-assembling peptides has been investigated as a route for the formation of functional nanostructures designed for specific applications. Here, we have modified the diphenylalanine (FF) peptide, previously shown to spontaneously form fibrous self-assemblies, with two organic chelating groups capable of coordinating various transition metals. We investigated the self-assembling behaviors of this peptide in coordination with several combinations of Pt(II), Re(I), or Rh(III) using Fourier transform infrared (FTIR) spectroscopy, circular dichroism (CD) spectroscopy, and scanning electron microscopy (SEM). SEM analysis indicated that both homo-metallated species of Pt(II) and Re(I) as well as the non-metallated species form fibrous self-assemblies. However, the heterometallic peptide coordinating Pt(II)and Rh(III) did not form distinguishable fibrous structures under identical conditions. We propose that the charge states of the metal centers may affect the self-assembly properties of these peptide compounds. Further investigation into possible self-assembling heterometallic dipeptides could be beneficial for the future development of more complex, metallated nanostructures.

Introduction:

Peptide-based compounds are desirable targets for the development of novel nano-materials due to their propensity to form self-assembled, supramolecular architectures. Short, aromatic peptides such as diphenylalanine (FF) exhibit particularly strong tendencies to self assemble; FF has been previously shown to self-assemble into discrete, robust nanotubes [1]. The biocompatibility of these peptide nanostructures, as well as the ability to modify the peptide backbone with numerous function groups, has given these compounds versatility and usefulness in a wide range of applications [2].

The incorporation of transition metals into the structure of self-assembling peptides may provide a route towards the development of more complex metallic nanostructures with novel properties. Recently, the FF structural motif has been incorporated into a Ru(II) complex, resulting in the first metallo-hydrogellator capable of redox-responsive self-assembly and gelation [$_3$]. The incorporation of multiple chelating functional groups capable of coordinating a broader range of transition metals into a self-assembling peptide could significantly increase the complexity of these nanostructures, and provide potential catalytic or fluorescent properties.

Here, we have developed a method for the incorporation of heterometallic complexes into the backbone structure of a self-assembling peptide. We modified the FF structural motif with two organic chelating groups capable of coordinating either Pt(II), Re(I), Rh(III), or Ru(II). This technique not only allows for the synthesis of heterometallic peptidic arrays, but also allows for the sequential addition of amino acid subunits to achieve peptide chains with more than two metal centers.

Experimental Procedure:

Metallated peptides were synthesized previously using either a conventional solution phase synthesis technique or a modified form of the Merrifield solid-phase synthesis technique [4]. One non-metallated and three metallated peptides studied here are shown in Figure 1.

SEM Analysis. A 0.1 mM sample stock solution was prepared by suspending 0.5 mg (0.3 μmol) of peptide in 3 mL acetonitrile (ACN). The suspension was sonicated for 30 s followed by heating at 50°C for one min; this process was repeated until the solid had fully dissolved. After 24 hr of incubation at 22°C, the solution was spotted onto a silicon substrate and visualized using a Hitachi SU8000 scanning electron microscope.

CD Analysis. Samples were prepared identically to SEM samples, with the addition of a 10-fold dilution to achieve a proper concentration for CD analysis. Their CD spectra were recorded on a JASCO Type J-820 spectropolarimeter at -10°C.

FTIR Analysis. Samples were prepared as pellets in solid KBr and their spectra were recorded using a Thermo Scientific model Nicolet 4700 Fourier transform infrared spectrometer.

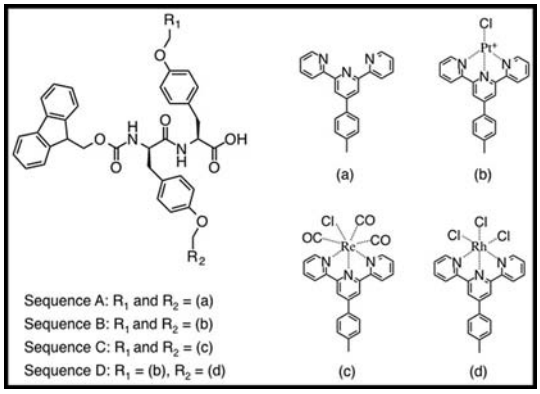

*Figure 1: Series of non-metallated (**A**) and metallated (**B**-**C**) peptides.*

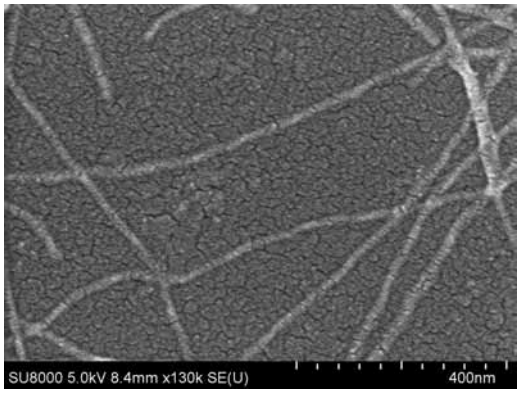

*Figure 2: SEM of non-metallated peptide (**A**) self-assemblies.*

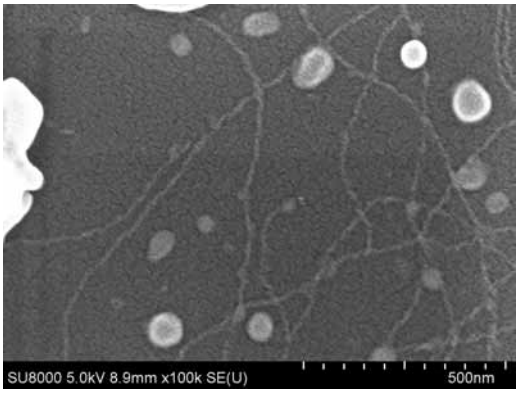

*Figure 3: SEM of Pt^{+}-Pt^{+} peptide (**B**) self-assemblies.*

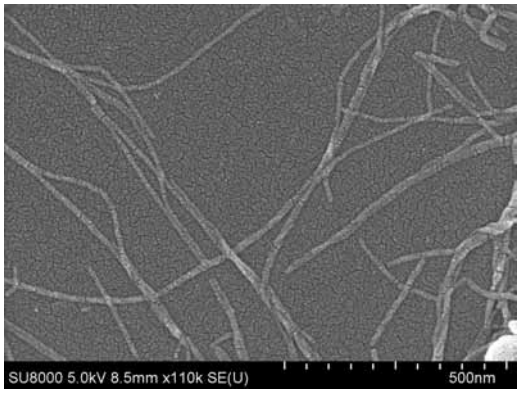

*Figure 4: SEM of Re-Re peptide (**C**) self-assemblies.*

Results and Conclusions:

All four peptide compounds were weakly soluble in ACN. After several hours of incubation at 22°C, the formation of solid aggregates was observed. SEM analysis indicated that sequences **A**, **B**, and **C**, but not **D**, formed fibrous assemblies shown in Figures 2-4. While the charge state of the metal centers was identical (either $^{+}1$ or 0) for **A**, **B**, and **C**, the charge state of the Pt(II) and Rh(III) in **D** were different ($^{+}1$ and 0, respectively). It is possible that the charge symmetry of the metal centers may affect the self-assembling properties of the compound, which may explain the absence of fibrous aggregates in the hetero-metallic species.

The non-metallated sequence (**A**) gave a relatively strong CD signal with a positive peak at 198 nm, while the CD signals of the metallated peptides were too weak to distinguish. Additionally, two strong bands between 1670-1690 cm^{-1} and 1607-1612 cm^{-1} in the infrared spectra of compounds **A**-**D** were observed. Previously studied FF-based nanostructures have characteristic IR stretching frequencies around 1630 cm^{-1}, attributed to peptide amide groups in the β-sheet conformation [1]. The absence of an amide stretch around 1630 cm^{-1} in the metallated peptides suggests that these monomers are not arranged in a β-sheet conformation.

Future Work:

Future work will investigate the conditions most appropriate for the formation of fibrous structures of hetero-metallated species. The ability to develop self-assembling peptides with hetero-metallic centers is useful for the development of more complex metallated architectures. Such compounds have not been reported previously, and may possess interesting catalytic or electronic properties. Additionally, field effect transistor measurements can be performed on homo-metallated dipeptides to measure the potential semi-conductive properties of these compounds.

Acknowledgements:

I would like to thank the Dr. Kentaro Tashiro and Reticular Materials Group for their guidance. I acknowledge the NSF and NNIN iREU Program for financial support, and the National Institute of Materials Science for hosting me.

References:

[1] Reches, M.; Gazit, E. Science 2003, 300, 625.
[2] Gazit, E. Chem. Soc. Rev. 2007, 36, 1263.
[3] Zhang, Y., et al., J. Am. Chem. Soc. 2013, 135, 5008.
[4] Vairaprakash, P., et al., J. Am. Chem. Soc. 2011, 133, 759.

Directed Self Assembly of Mixed Nanowire Populations via Lithographic Microwells

Allison Wustrow
Chemistry, University of California Berkeley

NNIN REU Site: Penn State Nanofabrication Laboratory, The Pennsylvania State University, University Park, PA
NNIN REU Principal Investigator: Christine Keating, Chemistry, The Pennsylvania State University
NNIN REU Mentor: David Kirby, Chemistry, The Pennsylvania State University
Contact: wustrow@berkeley.edu, djk291@psu.edu, keating@chem.psu.edu

Introduction:

Vertical nanowire arrays can be used for both energy harvesting and storage. Using assembly to create such arrays allows two populations to be mixed together, while standard fabrication limits the product to a single material. However in the absence of applied fields [1] or controlled drying conditions [2], nanowires typically assemble parallel to the surface, forming horizontal arrays. The Keating group has worked with anisotropic particles, called partially etched nanowires, which form arrays where up to 70% of wires were vertically oriented on a planar surface when their internal asymmetry was tuned to optimize van der Waals and electrostatic interactions [3]. Array quality was increased to nearly 100% standing when microwells were used to direct assembly [4].

A similar approach was used for this work to generate vertical arrays of single component nanowires that lacked the material anisotropy used previously. Wire-wire interactions, such as van der Waals forces, which depend on the composition of the nanowire, were also studied by mixing wires of two different compositions.

Understanding these assemblies could help with design of reconfigurable materials.

Experimental Fabrication:

Nanowires were made by templated electrodeposition [5] in porous alumina membranes. Silver (Ag, 300 nm) was evaporated on to the membrane (Whatman). Plating solutions of silver cyless R, orotemp 24, and pallaspeed VHS_RTU (Technic inc.) were used to make palladium and gold wires with diameters around 300 μm, as determined using transmission electron microscopy.

The evaporated Ag layer, which served as a working electrode, was dissolved in nitric acid, and the alumina template was dissolved in sodium hydroxide, freeing the wires into suspension.

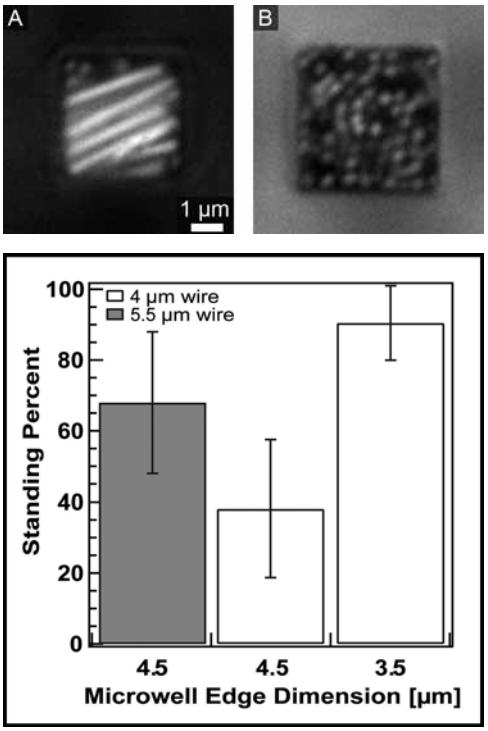

Figure 1, top: Assembled nanowires after one hour. (A) shows 4 µm wires in a 4.5 µm well which have a low standing percentage. (B) shows 5.5 µm wires in a similar well which have a high standing percentage.

Figure 2, bottom: Standing percentage for different particle lengths in different sized wells. At least 480 wells were counted for each data point.

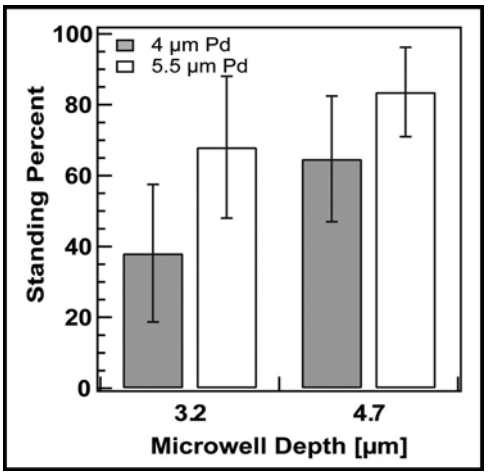

Figure 3, top: Standing percentages for nanowires assembled in microwells of different depths. At least 900 wells were counted for each data point.

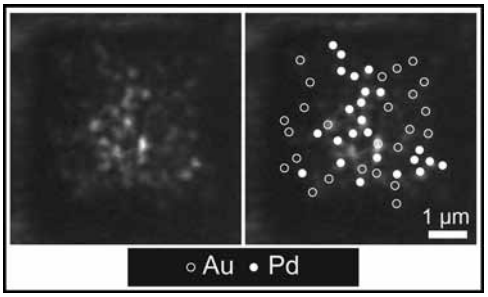

Figure 4, bottom: Optical micrograph of a binary nanowire assembly. Images are an overlay of reflectivity information collected at wavelengths of 488, 514, and 543 nm. A ratio of the intensities was used to determine the assignments as labeled in the right image.

Nanowires were cleaned by repeated centrifugation in sodium hydroxide or ethanol, and were ultimately suspended in deionized water. Particles were coated with a silica shell using a modified Stober process [3]. Wire concentration was determined using a hemocytometer. Microwells were made using SPR 955 photoresist (Microchem).

Assembly:

An assembly chamber was created by isolating a selection of microwells using a polydimethylsiloxane spacer (DOW Corning). Enough particles to form a single monolayer of standing wires were rinsed in deionized water. The suspension was sonicated and added to the assembly chamber, where it was allowed to settle for one hour before imaging. Standing percentage was determined using previously published methods in which image analysis software distinguished standing from laying down wires [3]. In binary mixture experiments, the wire material was determined by comparing the reflected light intensity for 488, 514, and 543 nm light.

Results:

Wire length affected standing percentage when well size was constant for palladium nanowires assembled into microwells. Longer wires in general had higher standing percentages (Figure 1). Palladium wires 4 μm in length assembled in 4.5 μm wells had 20 percentage points lower standing than 5.5 μm wires (Figure 2). Gravity drove the wires into the wells, where the longer wires were unable to fit in the horizontal conformation, and thus form vertical arrays. Microwell size also affected standing percentage. When 4 μm wires were assembled in 4.5 μm wells, standing percentage was higher than when the same wires were assembled in 3.5 μm wells (Figure 2). Deeper wells could support the wires along the entire length of the 4 μm wires, as well as a larger fraction of the 5.5 μm wires. This extra support raises the standing percentage in the wells regardless of nanowire length.

After vertical array quality had been optimized, binary nanowire mixtures were assembled. For these experiments, gold wires 4 μm in length were mixed with 5.5 μm palladium wires. These wires had the potential to exhibit interesting physical behavior due slight differences in their Hamaker constants (i.e. van der Waals interactions). Here we successfully assembled mixtures of these particles into vertical arrays and using optical microscopy we were able to distinguish the two populations via their differing reflectivities. Further study is needed to explore potential phase behavior.

Conclusions and Future Directions:

Nanowires were assembled vertically in microwells by controlling the particle and microwell dimensions. Mixtures of two types of wires were placed in the wells and identified by the differing reflectivities of the metals. As more samples are examined, it will be possible to study the phase behavior caused by the differences in inter-wire interactions, allowing generation of phase diagrams to describe the system. Understanding the mixing and demixing of vertical nanowire arrays will allow for the development of reconfigurable materials.

Acknowledgements:

This work was primarily supported by funding from the NNIN Research Experience for Undergraduates Program and the National Science Foundation. Acknowledgement is also made to the Donors of the American Chemical Society Petroleum Research Fund (ACS PRF 50888-ND10). We appreciate the use of the Huck Institute of Life Sciences Electron Microscopy Facility. This publication was supported by the Pennsylvania State University Materials Research Institute Nanofabrication Lab and the National Science Foundation Cooperative Agreement No. ECS-0335765.

References:

[1] Loaiza, Ó. A., et al. Angew. Chem. Int. Ed, 46, 1508-1511, 2007.
[2] Zhang, X., et al. J. Phys. Chem. C., 113, 5947-5951, 2009.
[3] Smith, B., et al. Small, 6, 781-787, 2011.
[4] Kirby, D., et al. Manuscript submitted to Part. Part. Syst. Charact.
[5] Nicewarner-Peña, S., et al. Science, 294,137-141, 2001.

Azobenzene Functionalized DNA for Light-Induced DNA Stringency

Hannah Zeitler
Physical Chemistry, Whitworth University

NNIN REU Site: NanoTech User Facility, University of Washington, Seattle, WA
NNIN REU Principal Investigator: David Ginger, Chemistry, University of Washington
NNIN REU Mentor: Yunqi Yan, Chemistry, University of Washington
Contact: hzeitler15@my.whitworth.edu, ginger@chem.washington.edu, yanyunqi@uw.edu

Abstract and Introduction:

Azobenzene functionalized deoxyribonucleic acid (DNA) and DNA modified gold nanoparticles (AuNP) are used to study light-induced DNA stringency, a method to distinguish perfectly matched DNA from partially matched DNA using light. To do this, AuNP are functionalized with DNA [1], and azobenzene modified DNA is attached to glass slides to use chip-based assays. The photoisomerization quantum yield of azobenzene, chemically attached with DNA molecules, is also measured in order to study the temperature's effect on azobenzene isomerization efficiency.

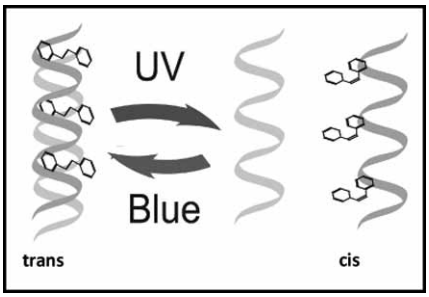

Figure 1: Azobenzene modified DNA switching between dsDNA and ssDNA with light. (See full-color version on inside cover.)

Azobenzene is an organic molecule that can photoisomerize between the *trans*- and *cis*-form. *Trans*-azobenzene can isomerize into the *cis*-form under UV light, and the reverse will happen under blue light. Azobenzene can be chemically attached to DNA [2], which will permit control over whether DNA is a double or single strand using light (Figure 1).

Complementary single-stranded DNA (ssDNA) will form double-stranded DNA (dsDNA) when azobenzene is in the *trans*-form. Under exposure to UV light, a properly formed dsDNA incorporating azobenzene modifications will denature into ssDNA, since the formation of *cis*-azobenzene will induce steric hindrance. Previous research has shown that azobenzene resists photoisomerization into the *cis*-form when it is attached to a perfectly matched dsDNA, as compared with when it is attached to a partially matched dsDNA [3]. This result explains the phenomenon that with the same amount of UV energy, perfectly matched dsDNA stays bound while partially matched dsDNA denatures. This difference in behavior allows light to be used to perform DNA hybridization stringency.

While previous studies have shown photo-controlled DNA stringency in solution, the focus of this summer's research was to attach DNA to a glass substrate and study its photoswitching properties.

Experimental Procedure:

To achieve chip-based DNA stringency, a glass substrate was functionalized with azobenzene modified DNA, 5′-/5Thio MC6-D/AAA AAA AAA TG/ iAzoBenz/ AA/iAzoBenz/ CT/iAzoBenz/ AA/iAzoBenz/ CG-3′. A silanized glass slide was covered with a hybridization chamber that was filled with succinimidyl 4-(p-maleimidophenyl)butyrate, SMPB, overnight. Azobenzene was added for six hours and bonded to the SMPB. Unbound SMPB was pacified with 6-mercapto-hexanol for thirty minutes.

A target strand of DNA was attached to the azobenzene DNA for two hours. The glass was exposed to UV light for two hours. Then DNA modified AuNP were inserted into the chamber for one hour. A silver enhancement solution was added for ten minutes so that the silver ions ionized around the AuNP creating a spot where the AuNP remained.

Quantum yield is a calculation based on how much *trans*-azobenzene has isomerized into *cis*-azobenzene divided by the number of photons [4]. To measure quantum yield, a solution of ssDNA containing azobenzene was prepared. The experimental apparatus for calculations consisted of an Agilent 8453 UV-Vis spectrometer, UV LEDS, a temperature controller, and a stirring plate. A photodiode was used to measure the UV light intensity before photoswitching. The DNA solution was placed in a cuvette and allowed to equilibrate in the apparatus without UV exposure for an hour. After the time elapsed, the solution was exposed to the UV light, and UV-Vis spectra were taken over the next hour at specific times. The data from the spectra was collected focusing on the 330 nm wavelength. This data was then analyzed with a curve-fitting program which created a numerical analysis of the quantum yield as the azobenzene transformed from *trans* to *cis*.

Result and Conclusions:

When looking at the glass slides that had been silver enhanced, a solid grey square was expected when a perfectly matched target strand of DNA was present. However, when it was a partial match, the intensity of the grey was expected to be less. This research focused on perfecting these steps to make the process more effective. To do this, the different steps were analyzed. From this, the importance of attaching the DNA in high quantities to the glass was understood. Otherwise, the AuNP could directly attach to the glass via non-specific interactions. This would create a false positive when the silver enhancer was used.

Another key factor was the age of the DNA attached to the glass (Figure 2 and Figure 3). From the figures, it is shown that the newer DNA allowed for a greater difference for observation of perfectly matched DNA compared to completely mismatched DNA. This shows that the older DNA began to break down and allowed the AuNP to directly attach to the glass.

The quantum yield was studied for A-azo, 5′-AAA AAA AAA /iAzoBenz/ AAA AAA AAA-3′, and T-azo, 5′-TTT TTT TTT/ iAzoBenz/TTT TTT TTT -3′. Research has shown that A-azo is more rigid than T-azo [5]. Because of the differing rigidity, the effect of temperature on the DNA strands was studied. A-azo at 29°C had a quantum yield of 0.044 ± 0.001, while at 37°C the quantum yield was 0.053 ± 0.00005. T-azo at 29°C had a quantum yield of 0.067 ± 0.014, while at 37°C the quantum yield was 0.064 ± 0.016. A-azo had a 19.5% increase in quantum yield at higher temperatures, and T-azo had a 5.1% decrease in quantum yield at higher temperatures.

As a result, it can be concluded that the higher temperatures have a greater effect on the more rigid DNA.

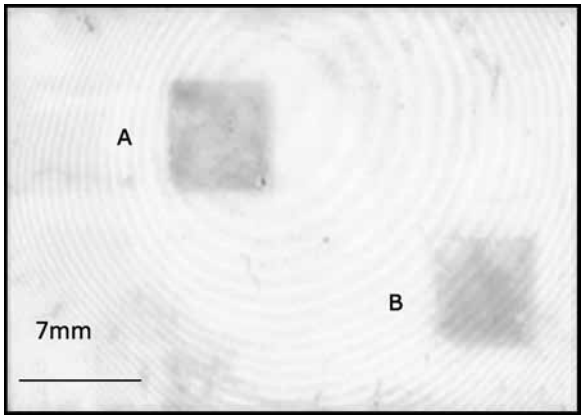

Figure 2: Old DNA; A) Perfectly matched DNA, and B) Mismatched DNA.

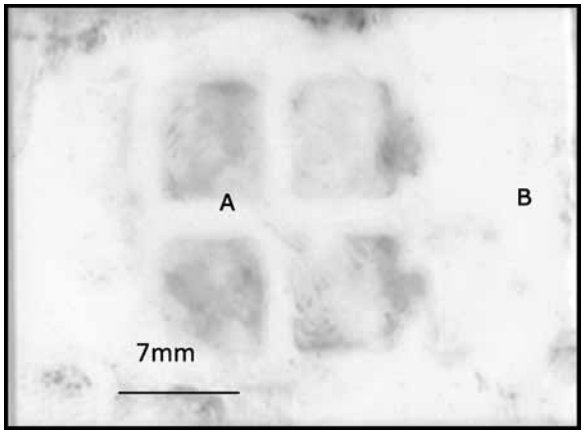

Figure 3: New DNA; A) Perfectly matched DNA, and B) Mismatched DNA.

Acknowledgments:

This researcher would like to acknowledge the NNIN REU Program funded by NSF as well as the Ginger lab, especially Yunqi Yan for her guidance as mentor and David Ginger as the Principal Investigator. Additionally, Mack Carter, as site coordinator, was a valuable resource.

References:

[1] Mirkin, C. et al. Nature, 382, 607, 1996.
[2] Asanuma, H., et al. Nature Protocols, 2, 203, 2007.
[3] Yan, Y.Q., et al. Nano Lett., 12, 2530-2536, 2012.
[4] Yan, Y., et al. Journal of the ACS, 135 (22), 8382-8387, 2013.
[5] Goddard, N. L., et al., Phys. Rev. Lett., 85, 2400-2403, 2000.